

CFD Modeling Analysis of a Martian Rotorcraft with Individual Blade Control^{1,2}

Paul Schulman*, Samuel-Hunter Berndt**, Christiahn Roman**, and Xiaobo Tan*

**Department of Electrical and Computer Engineering
Michigan State University, East Lansing, MI 48824 USA
(e-mail: schulm14@msu.edu, xbtan@msu.edu)*

***Jet Propulsion Laboratory, California Institute of Technology, Pasadena, CA 91109 USA
(e-mail: samuel-hunter.berndt@jpl.nasa.gov, christiahn.roman@jpl.nasa.gov)*

Abstract: Computational fluid dynamics (CFD) analysis was conducted on a proposed blade root-actuated Individual Blade Control (IBC) system for future Martian rotorcraft. IBC offers many potential benefits to rotary-winged exploration of Mars, including precision control of rotor blade forces. This study seeks to provide an estimate of rotor blade force and system power as a basis for concept feasibility analysis and experimental prototyping. ANSYS Fluent was used to compute blade pitching moment, lift, and drag under various feathering waveforms, amplitudes, biases, and frequencies. It is determined that the rapid feathering characteristic of IBC has a non-negligible impact on blade forces. It is also found that actuators with power ratings on the order of 10^1 W are likely sufficient for blade actuation on Martian rotorcraft.

Keywords: rotorcraft, exploration, Mars, individual blade control, actuators, CFD.

1. INTRODUCTION

The Mars Helicopter, Ingenuity, completed the first flight on another planet on April 19th, 2021 and has logged over 50 successful flights since. Ingenuity features a pair of two-bladed rotors, each controlled by its own electrically actuated swashplate. The 1.2 m diameter rotors spin at speeds of up to 2,800 RPM^[1]. Other Martian rotorcraft have also been proposed, including the Mars Sample Recovery Helicopters and Mars Science Helicopter, each having rotor diameters of approximately 1.2 m. This is because larger rotors are limited due to uncontrolled blade flapping modes, which represents a major constraint on Martian rotorcraft.

When a helicopter blade flaps, the up and down motion produces a change in the blade angle of attack. This change in angle of attack creates a force opposing the flapping motion of the blade. On Earth, this opposing force is sufficient to dampen the flapping motion. The Martian atmosphere, however, has a density of approximately 1% that of Earth's and does not provide sufficient damping^[1]. If the rotor blades are allowed to flap at high amplitudes, structural failure will occur. Currently, control bandwidth must be limited, and blade rigidity and mass must be increased to avoid excessive

flapping of the blade. For rotors larger than the current state-of-the-art, acceptable control bandwidth would require a blade mass that is too large, thus presenting an upper limit on rotor size for Martian rotorcraft. Resolving this problem requires the creation of either stiffer light-weight blade materials to increase the blades' natural frequencies or a blade flap damping system. In this work we propose a novel solution to dampen blade flap using Individual Blade Control (IBC).

Helicopters derive their motion through dissymmetry of lift, that is, different sections of the rotor disk produce different magnitudes of vertical force, resulting in a horizontal component of the net force vector. Dissymmetry of lift is created across the rotor system by pitching, or "feathering", each blade as a function of its position around the disk. Traditional helicopters, including the Mars Helicopter, accomplish this blade pitch actuation with a mechanical swashplate system, shown in Figure 1. The swashplate is a tilting assembly that transfers orientation from the static frame to the rotating frame and is rigidly attached to the blades, causing them to pitch as they rotate around the rotor disk. Because the swashplate is a rigid, planar disk, blades are limited to a once-per-revolution (1/rev) sinusoidal pitch change and are coupled by phase to the other blades. Unfortunately, this limits the adaptability of blade pitch required for countering aerodynamic perturbations or manipulating transient forces.

In contrast, IBC is a rotor control technique by which each blade's pitch is actuated independently of the others. IBC can

1 Paper presented at the 2023 Modeling, Estimation, and Control Conference (MECC 2023), Lake Tahoe, NV, Oct. 2-5. Paper No. MECC2023-124.

2 This research was supported by the Jet Propulsion Laboratory, California Institute of Technology, under a contract with the National Aeronautics and Space Administration (80NM0018D0004).

independently actuate the blades multiple times per revolution in an arbitrary waveform, thus allowing precise control of transient blade forces. IBC has shown the ability to reduce rotor vibrations, noise, energy consumption, and blade stresses^[2], as shown in simulation, wind tunnel testing, and manned flights^{[3][4][5][6]}. IBC can also be implemented in many forms, such as morphing blades, active trailing-edge flaps, and blade-root actuation. In particular, the blade-root actuation method, the focus of this work, places pitch-altering actuators at the root of each blade and eliminates the swashplate.

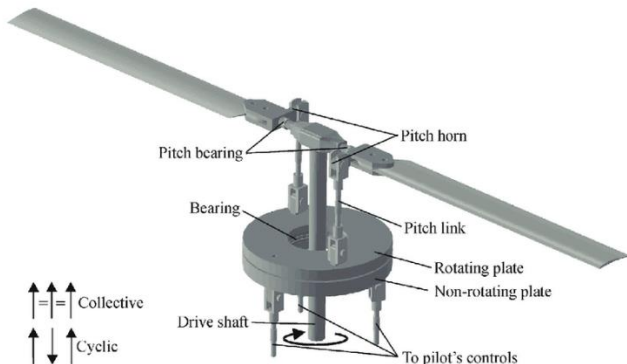


Fig. 1. Diagram of a swashplate^[7].

Despite the aforementioned efforts, there has been little research on blade-root actuation IBC for unmanned aerial vehicles (UAVs) or for Martian rotorcraft. A key difference of IBC on the UAV scale is the high speed, low mass, and compact size of the rotor system, which is conceptualized in Figure 2. Consequently, implementation of IBC on Martian UAVs requires centimeter-scale high-speed actuators not typically studied in the context of IBC. Saxena and Chopra implemented 10 mm diameter rotating-frame actuators at a frequency of 40 Hz on trailing-edge flap IBC test platforms^[8]. However, for the proposed application on Martian rotorcraft, it is expected that actuation frequencies will be upwards of 100 Hz. Furthermore, no information is available on the performance of IBC in the Martian atmosphere, where flight itself is an emerging science.

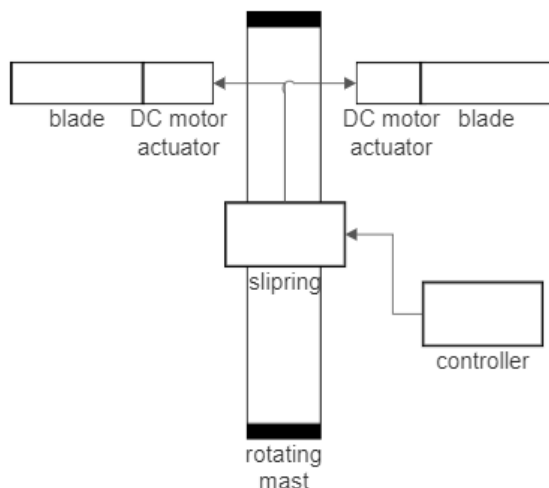


Fig. 2. Illustration of a simple blade root-actuated IBC rotor. The thin atmosphere, small blade size (relative to manned rotorcraft), and high rotor speed characteristic of flight on Mars leads to operating conditions with ultra-low Reynolds numbers. Noonan and Bingham reported Reynolds numbers of 3×10^6 to 6×10^6 on manned, terrestrial rotorcraft^[9]. The Reynolds numbers for the Mars Helicopter are estimated to be between 1×10^4 and 2.5×10^4 ^[10]. Comparable flight conditions on Earth are those of insects, small birds, and micro air vehicles (MAVs), in which Reynolds numbers on the order of 10^4 ^[11].

The objective of this study is to predict the achievable ranges of blade forces, to estimate hardware performance requirements, and to advise on the design of IBC-enabled blade flap damping systems for Martian rotorcraft. This will be accomplished by exploring the impacts of blade angle of attack, pitching angular velocity, pitching angular acceleration, and pitching waveform on power requirements for blade-root actuators and rotor-drive motors during rapid IBC feathering in the Martian atmosphere. The achievable ranges of blade forces will define the system's ability to dampen blade flap. In this work, a CFD study is conducted in ANSYS Fluent to estimate blade forces under various feathering frequencies, amplitudes, pitch bias (known as "collective", or the average angle of attack), and waveforms. These blade forces are used to estimate the maximum transient power of the IBC actuators and the time-averaged power consumption of the IBC and rotor drive systems.

2. APPROACH

2.1 Blade Geometry and Mesh

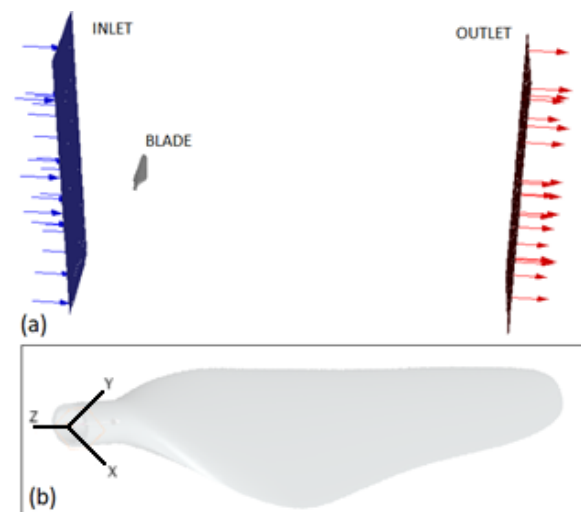


Fig. 3. (a) The inlet, outlet, and blade position and (b) the blade geometry, datum, and axes.

A rotor blade with properties like those of the Mars Helicopter was modeled and is shown in Figure 3. A low-Reynolds number airfoil, CH 10-48-13, was used from root to tip, excluding blending zones and the cylindrical root. The blade's

pitching axis (z -axis) is coincident to the longitudinal centerline of the cylindrical root. The blade planform matches that of the Mars Helicopter^[12], though no longitudinal twist is applied. The moment of inertia about the pitching axis is $1.73 \times 10^{-5} \text{ kg} \cdot \text{m}^2$. The blade is encased in a 4.2 m by 2.8 m by 1.0 m rectangular fluid environment, with the blade feathering axis located 0.7 m from the flow inlet. The mesh is made of 1,087,191 tetrahedron elements. The maximum face size is $8.88 \times 10^{-3} \text{ m}^2$, the minimum face size is $1.02 \times 10^{-8} \text{ m}^2$, and the minimum edge length is $1.86 \times 10^{-4} \text{ m}$.

2.2 Fluent Setup

Inlet flow was set as a linear gradient from 2 m/s at the blade root to 177 m/s at the tip. The fluid was matched to the Mars atmospheric conditions: density of 0.017 kg/m^3 , dynamic viscosity of $1.130 \times 10^{-5} \text{ N} \cdot \text{s/m}^2$, and temperature of 223 K. Blade feathering was achieved with a user-defined function for rigid body motion. A viscous k - ω SST model with Low Reynolds Number corrections was used. Validation of simulation results was conducted by varying simulation models and variables and observing the behavior of the results. First, three viscous models were tested, including the k - ϵ , Spalart-Allmaras, and k - ω SST models. No significant change was observed in the results, indicating a stable setup. Next, the timestep was varied from larger to smaller. It was noticed that below a certain timestep, the results did not change. Below an even smaller timestep, the results exhibited discontinuities expected when a timestep is too small. Suitable timesteps were chosen within this range.

2.3 Static Tests

Tests were completed without blade feathering in order to determine the aerodynamic properties of the blade and to establish a baseline case in which feathering plays no role in blade performance. For the static case, 250 timesteps of 0.001 s were executed for a total of 0.25 s, which allowed sufficient time for a steady solution to develop. Pitching moment, lift, and drag data was produced at each angle of attack. Center of pressure on the xz -plane intersecting with the pitching axis was determined. Data was gathered for each angle of attack between 0° and 20° inclusive for a total of 21 simulation runs.

2.4 Dynamic Tests

The main efforts of the study were the tests implementing blade motion. For the dynamic cases, 5,000 steps of $5 \times 10^{-5} \text{ s}$ were executed for a total of 0.25 s, which allowed sufficient time for a repeating transient solution to develop. Five test sets were carried out, each imparting a different pitching motion on the blade. Each test set included tests at pitching frequencies of 1, 2, 4, 6, and 8/rev. The five test sets are as follows, described by waveform, peak-to-peak amplitude, and bias (collective):

1. Sinusoidal waveform, 10° amplitude, 5° bias.
2. Sinusoidal waveform, 2° amplitude, 1° bias.
3. Sinusoidal waveform, 2° amplitude, 5° bias.
4. Skewed sinusoidal waveform, 2° amplitude, 5° bias.
5. Quadratic waveform, 2° amplitude, 5° bias.

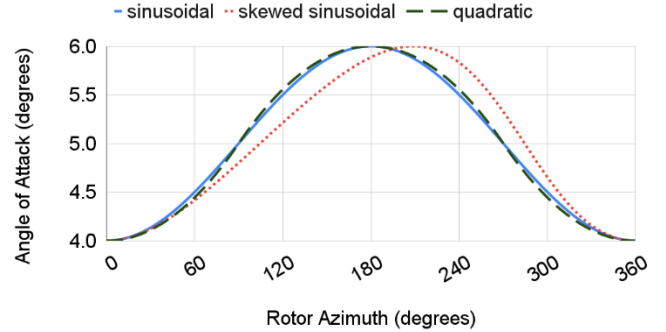


Fig. 4. Blade angle of attack as a function of rotor azimuth at a frequency of 1/rev, amplitude of 2° , bias (collective) of 5° , for three different waveforms.

Figure 4 illustrates the three waveforms studied in this work. The sinusoidal waveform, which also describes traditional swashplate systems at a 1/rev frequency, is defined by

$$AOA(t) = -\frac{\theta_{IBC}}{2} \cdot \cos(n \cdot \omega_{rotor} \cdot t), \quad (1)$$

where AOA is the blade angle of attack in radians, t is the time in seconds, θ_{IBC} is the blade pitching amplitude in radians, n is the pitching frequency per rotor revolution (1/rev), and ω_{rotor} is the rotor speed in rad/s.

The skewed sinusoidal waveform is approximated by

$$AOA(t) = \frac{0.494708}{-0.25} \tan^{-1} \left(-0.25 \frac{\sin(f)}{1 - c \cdot \cos(f)} \right) \quad (2)$$

where f is defined as

$$f = \omega_{rotor} \left(t - \frac{0.006219}{n} \right). \quad (3)$$

This waveform was considered after it was observed during testing that symmetric upward and downward pitching produced asymmetric results, with the upward pitching motion producing higher forces than the downward pitching motion. In an effort to minimize the maximum transient torque, the waveform was skewed by a factor of 25% towards the down pitch, leading to a faster down-pitch and slower up-pitch than the unskewed waveform.

The quadratic waveform is defined by

$$AOA(t) = \left(\frac{\theta_{IBC}}{2} \right) + \left(\frac{4\theta_{IBC}}{\pi^2} \right) \cdot \text{sgn}(\cos(n \cdot \omega_{rotor} \cdot t)) \cdot \left(\frac{\sin^{-1}(\sin(n \cdot \omega_{rotor} \cdot t))^2}{2} - \frac{\pi^2}{64} \right). \quad (4)$$

This waveform was considered after it was observed that the inertial moment during rapid pitching of the blade was much larger than the aerodynamic moment. Thus, a waveform that minimized maximum angular acceleration was sought. This was achieved by using a waveform that produced constant alternating angular acceleration with no peaks or valleys, at the consequence of having an infinite angular jerk.

2.5 Post-processing

The primary considerations for actuator performance are maximum torque, maximum angular velocity, maximum power, and time-averaged power. The torque about the pitching axis is computed as the sum of the blade's propeller moment, inertial moment, and aerodynamic moment. The propeller moment is the tendency of the blade's center of gravity to align with the plane of rotation and is computed by

$$M_{propeller} = I_{total} \cdot \omega_{rotor}^2 \cdot AOA(t), \quad (5)$$

where $M_{propeller}$ is the propeller moment in N-m and I_{total} is the total moment of inertia in kg-m². Moment of inertia is taken as the sum of the blade inertia, 1.73×10^{-5} kg-m², and the actuator rotor inertia, 1.08×10^{-7} kg-m², about the blade's pitching axis. The inertial moment is the blade's tendency to resist the pitching motion and is computed by

$$M_{inertial} = I_{total} \cdot \alpha(t), \quad (6)$$

where $M_{inertial}$ is the inertial moment and α is the pitching angular acceleration in rad/s². The aerodynamic moment is the result of air flow over the blade and is determined by simulation. Blade actuator power is determined by multiplying the blade's feathering (angular) velocity by the sum of moments acting on it. Per-blade rotor drive power is determined by multiplying the rotor velocity by its torque, where the torque is determined by multiplying the transient blade drag by the average center of pressure as measured in the negative direction from the blade root.

3. RESULTS

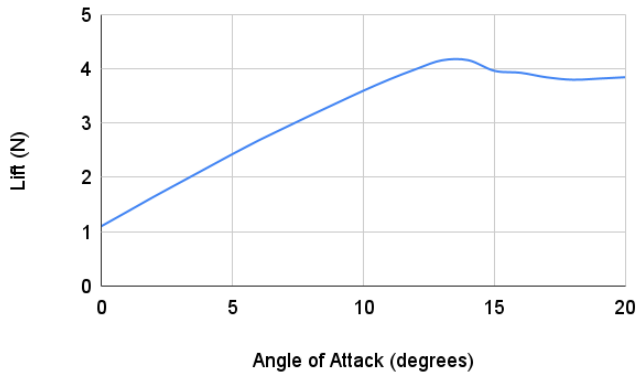


Fig. 5. Blade lift at fixed angles of attack.

Figure 5 shows the blade lift at different fixed angles of attack. The blade center of pressure moves from 0.007 m at 0° angle of attack to 0.000 m at 10° angle of attack in the x direction from the pitching axis. The center of pressure is near constant in the z direction at about 0.414 m from the blade root. It can be observed that the lift remains within an order of magnitude of the Mars Helicopter blade of approximately 1 N per blade at a hover. Furthermore, lift is observed to increase at a near constant rate between 0° and 10° angle of attack, the maximum feathering range tested in the dynamic cases.

Figure 6 shows that the peak pitching moment and lift increase with feathering frequency and that peaks occur at shifted angles of attack. This indicates that the blade center of pressure moves as a function of the pitching condition. Furthermore, this demonstrates that feathering frequency is an important factor in determining blade forces. In fact, under 2°, 4/rev actuation, peak moment and lift increased by 32% and 7% respectively over the values calculated from the static data.

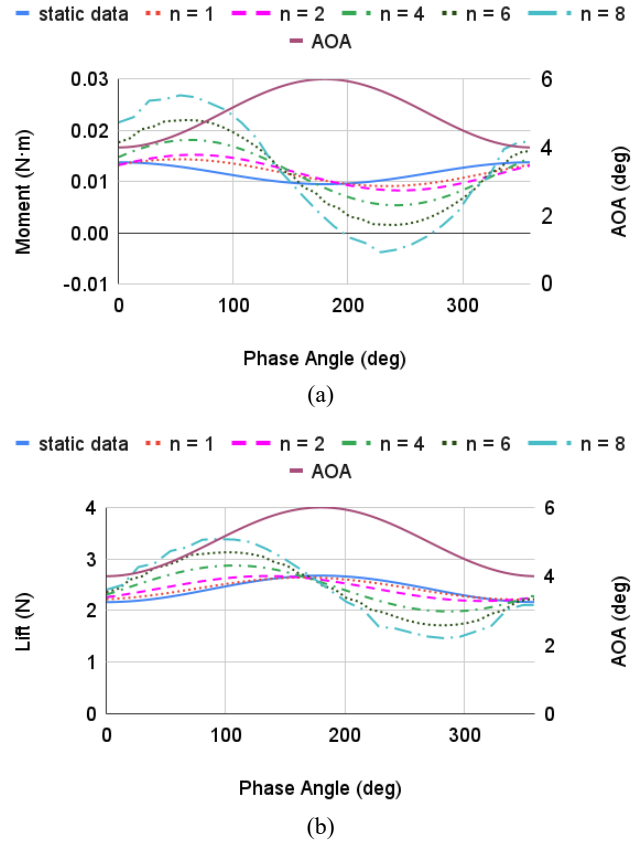


Fig. 6. Blade pitching moment (a) and lift (b) over a single actuation cycle under a sinusoidal waveform with 2° amplitude, 5° bias, and various frequencies.

Figure 7 shows the average power draw of the blade-root actuators and rotor drive motor per blade. It can be observed that actuator power and rotor drive power scale similarly for all actuation conditions, reaffirming that blade pitching moment and drag are coupled. The drastic difference between average and peak actuator power can be attributed to regeneration of power due to the inertia of the blade as it slows and begins to pitch in the opposite direction. Real-world energy losses would likely increase the average power draw.

Figure 8 gives the maximum transient power requirement of the blade-root actuators under the various test cases. It can be observed that sinusoidal actuation requires the lowest actuator power rating of the tested waveforms when actuation amplitude is held constant. While the quadratic waveform reduces the inertial moment, the sharper change in angular velocity produces a higher aerodynamic moment, canceling

out any benefit hoped to be gained. It can also be observed that pitch bias has little effect on the maximum transient power. Finally, it can be observed that, when 2° pitching amplitudes are applied at an up to 8/rev frequency, or 10° amplitudes at a traditional cyclic frequency of 1/rev, actuator power requirements remain on the order of 10¹ W.

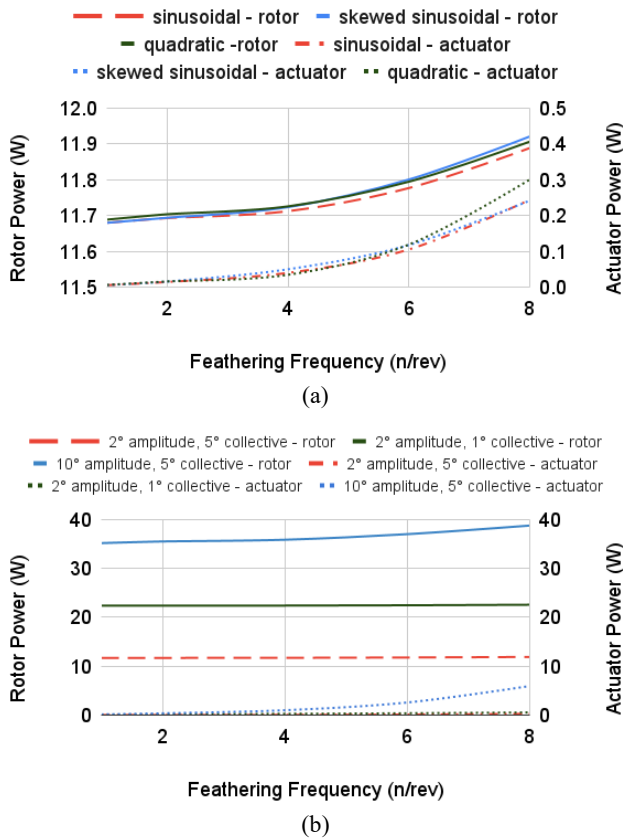


Fig. 7. Average power consumption of blade-root actuators and rotor drive motor calculated per-blade, at a 2° amplitude and 5° bias with varying waveforms (a) and a sinusoidal waveform with varying amplitudes and bias (b).

Figure 9 shows the lift produced for each test case. It can be observed that the average lift changes only as a result of bias (collective) and does not change as a result of amplitude or waveform. It can also be observed that waveform, amplitude, bias, and frequency affect the maximum transient lift, with the quadratic waveform producing the highest maximum lift when other factors are held constant.

Figure 10 shows the ability of each pitching condition to generate a change in vertical force (maximum transient lift minus minimum transient lift) as a function of the system power draw. For the 2° amplitude cases, it can be observed that a higher pitching frequency leads to a larger change in vertical force with a minimal increase in power draw. A 10° pitching amplitude produces higher changes in lift but does so at much higher power draws. Finally, it can be observed that these results vary relatively little across the tested waveforms.

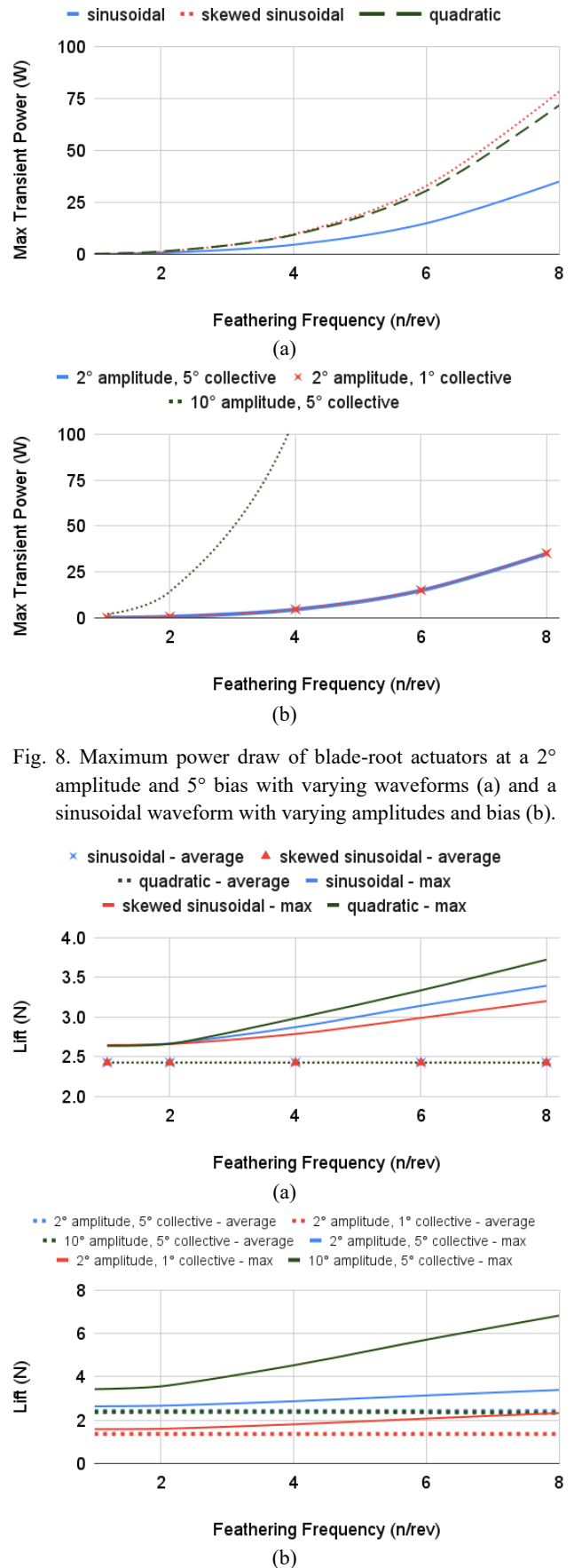


Fig. 8. Maximum power draw of blade-root actuators at a 2° amplitude and 5° bias with varying waveforms (a) and a sinusoidal waveform with varying amplitudes and bias (b).

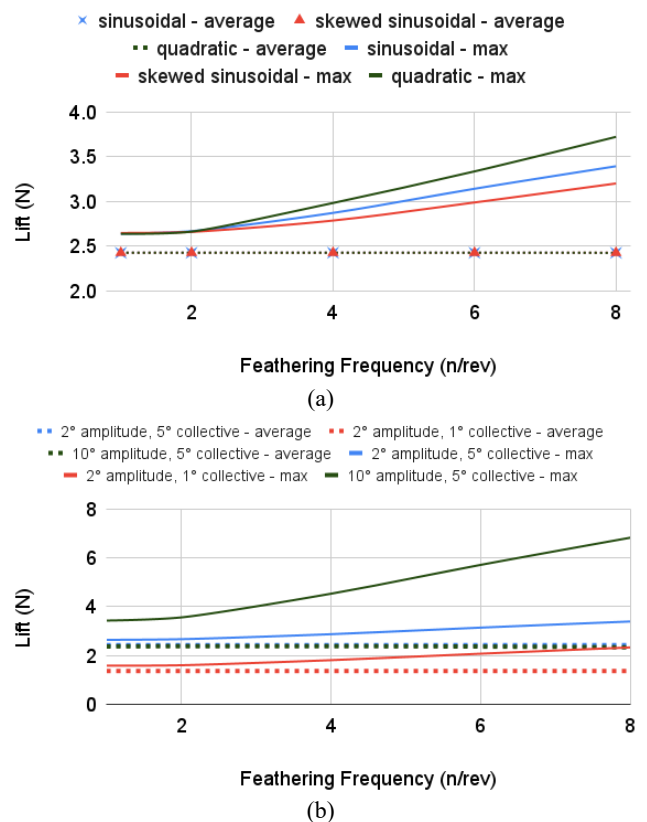


Fig. 9. Average and maximum lift per-blade at a 2° amplitude and 5° bias with varying waveforms (a) and a sinusoidal waveform with varying amplitudes and bias (b).

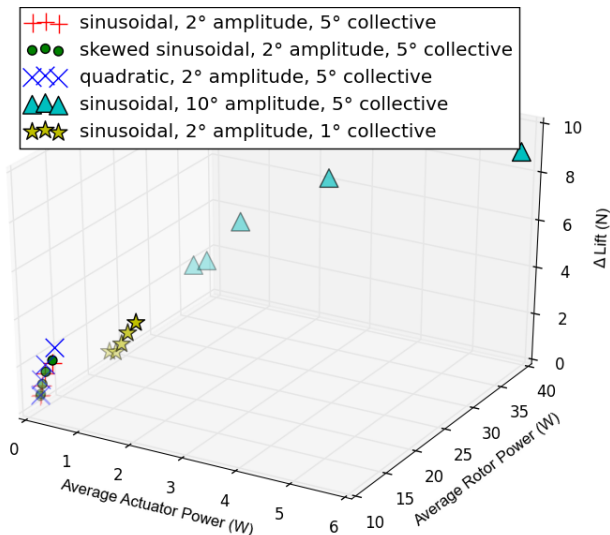


Fig 10. Change in lift per actuation for each test case plotted against system power draw. A darker shade indicates a higher frequency, with data displayed at 1/rev, 2/rev, 4/rev, 6/rev, and 8/rev for each test set.

4. CONCLUSIONS AND FUTURE WORK

This work investigated rotor blade forces and system power of a theoretical Individual Blade Control Martian rotorcraft. We found that sinusoidal actuation performed better than the other tested waveforms in regard to transient blade actuator power. Under such a condition, it was predicted that a 25 W actuator was capable of 1/rev cyclic input at 10° and up to 6/rev IBC input at 2°. Time-averaged blade actuator and rotor drive power were found to vary little with feathering frequency, but greatly with feathering amplitude. It was also predicted that per-blade peak-to-peak lift changes of 2 N are achievable. Furthermore, it was found that peak transient actuator power and center of pressure varied with feathering frequency. These results indicate that the proposed IBC system may be within the capabilities of current hardware, that a useful force gradient can be developed, and that aerodynamic effects of IBC actuation waveforms will necessitate additional analysis when compared to traditional swashplate systems.

Future work will focus on the inclusion of transient inlet flow and rotor blade deformation in order to capture aerodynamic perturbations and blade flapping modes which are limitations of the present work. We also plan to conduct experiments to validate the blade properties in ultra-low Reynolds number flow and to investigate the real-world performance and losses of commercial off-the-shelf actuators in order to overcome the accuracy limitations associated with computer modeling.

REFERENCES

[1] Grip, H.F., Johnson, W., Malpica, C., Scharf, D.P., Mandic, M., Young, L., Allan, B., Mettler, B., and Martin, M.S., (2017). Flight dynamics of a Mars helicopter. Published on the NASA Technical Report Server, DOCID: 20210007745.

[2] Jacklin, S. A., Swanson, S., Blaas, A., Richter, P., Teves, D., Niesl, G., Kube, R., Gmelin, B., and Key, D. L., (2020). Investigation of a helicopter Individual Blade Control (IBC) system in two full-scale wind tunnel tests: Volume I. Published on the NASA Technical Report Server, DOCID: 20205003457.

[3] Park, J.-S., Kim, D.-H., Chase, S., Lee, Y.-L., Go, J.-I., (2019). Vibration and performance analyses using individual blade pitch controls for lift-offset rotors. International Journal of Aerospace Engineering, Article ID 9589415.

[4] Norman, T.R., Theodore, C., Shinoda, P., Fuerst, D., Arnold, U.T.P., Makinen, S., Lorber, P., and O'Neill, J., (2009). Full-scale wind tunnel test of a UH-60 Individual Blade Control system for performance improvement and vibration, loads, and noise control. American Helicopter Society 65th Annual Forum.

[5] Spletstoesser, W. R., Shultz, K.-J., van der Wall, B., Buchholz, H., Gembler, W., and Niesl, G., (2000). Helicopter noise reduction by Individual Blade Control (IBC): selected flight test and simulation results. RTA - AVT Symposium, Number 30. Published on the Defense Technical Information Center, DOCID: ADP011125.

[6] Arnold, U.T.P., and Furst, D., (2005). Closed loop IBC results from CH-53G flight tests. Aerospace Science and Technology, Volume 9, pp. 421-435. DOI: 10.1016/j.ast.2005.01.014.

[7] Rotaru, C. and Todorov, M., (2017). Helicopter Flight Physics. Flight Physics – Models, Techniques and Technologies. InTech. DOI: 10.5772/intechopen.7156.

[8] Saxena, A. and Chopra, I., (2020). Wind tunnel testing of a swashplateless rotor with compact brushless motor actuated flaps for primary control. Journal of the American Helicopter Society, Volume 65, Number 1, pp. 1-6. DOI: 10.4050/JAHS.65.012010.

[9] Noonan, K.W., and Bingham, G.J., (1980). Aerodynamic characteristics of three helicopter rotor airfoil sections at Reynolds numbers from model scale to full scale at Mach numbers from 0.35 to 0.90. Technical publication. Published on the NASA Technical Report Server, DOCID: 19800023826.

[10] Koning, W.J.F., Romander, E.A., and Johnson, W., (2018). Low Reynolds number airfoil evaluation for the Mars Helicopter rotor. Presented at the American Helicopter Society International 74th Annual Forum and Technology Display. Published on the NASA Technical Report Server, DOCID: 20180008702.

[11] Alam, M.M., Zhou, Y., Yang, H.X., Guo, H., and Mi, J., (2009). The ultra-low Reynolds number airfoil wake. Experimental Fluids 48, pp. 81-103. Springer. DOI: 10.1007/s00348-009-0713-7.

[12] Pipenberg, B.T., Keenoon, M., Tyler, J., Hibbs, B., Landberg, S., Balaram, B., Grip, H.F., and Pempejian, J., (2019). Design and fabrication of the Mars Helicopter rotor, airframe, and landing gear system. AIAA Scitech 2019 Forum. DOI: 10.2514/6.2019-0620.